

Theoretical thermodynamics and practical kinetics studies of oxygen desorption from Co_3O_4 -5 wt% Al_2O_3 and Co_3O_4 -5 wt% Y_2O_3 composites

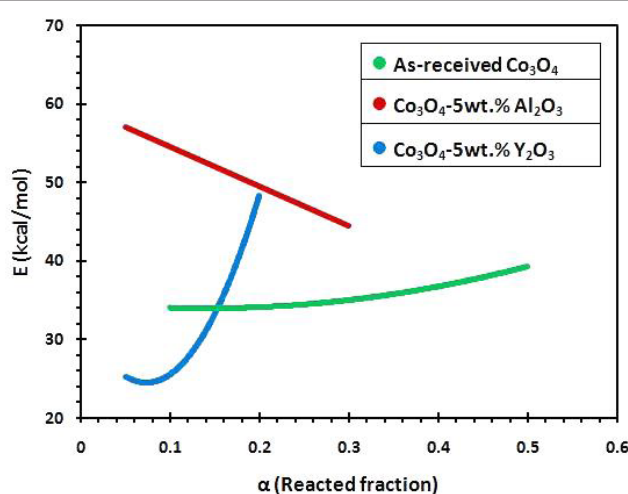
Azin Hasanvand, Mehdi Pourabdoli*

Department of Metallurgy and Materials Engineering, Hamedan University of Technology, Hamedan, Iran

HIGHLIGHTS

- Effect of thermodynamic parameters on the cobalt oxide redox process was studied.
- Isothermal reduction kinetics of Co_3O_4 containing alumina and yttria was investigated.
- Reduction activation energy of Co_3O_4 , Co_3O_4 -5% Al_2O_3 , and Co_3O_4 -5 % Y_2O_3 was calculated.

GRAPHICAL ABSTRACT



ARTICLE INFO

Article history:

Received 26 October 2018

Revised 28 December 2018

Accepted 15 January 2019

Keywords:

Cobalt oxide
Reduction
Activation energy
Thermal energy
Storage

ABSTRACT

Cobalt oxide is a candidate material for thermochemical heat storage via reversible reduction and re-oxidation reactions. In this research, the relationship between Gibbs' free energy (ΔG) with reaction temperature (T) and oxygen partial pressure (P_{O_2}) and the relationship between equilibrium temperature (T_e) and P_{O_2} were investigated theoretically. It was found that an increase in reduction temperature decreases the reduction ΔG . Also, increasing P_{O_2} increases the T_e and reduces ΔG . In addition, isothermal reduction kinetics of Co_3O_4 - 5wt% Al_2O_3 (CA) and Co_3O_4 - 5wt% Y_2O_3 (CY) were investigated at various temperatures (1040-1130°C) by thermogravimetric analysis. Results showed that the CA sample desorbs more oxygen than the CY sample in similar conditions. A model-free method was used to calculate the reduction activation energies. It was found that activation energy required for reduction of CA and CY samples, depending on conversion fraction (α), is in the range of 40-65 kcal/mol and 25-50 kcal/mol, respectively. Furthermore, results showed that the reduction activation energy of CA and CY samples decreased and increased as the conversion fraction (α) increased, respectively. The difference in the performance of alumina and yttria additions on the reduction of cobalt oxide was attributed to their ionic radii difference, the ability to create new compounds with different decomposition temperatures, and their different effect on the sintering of cobalt oxide particles.

* Corresponding author: Tel.: +9881-38411445; Fax: +9881-38380520; E-mail address: mpourabdoli@hut.ac.ir

1. Introduction

Increasing fossil fuel consumption increases the greenhouse gas emissions that result in air pollution and climate change. Therefore, newer technologies to produce clean energy to reduce fossil fuels consumption and air pollution are required. One of these technologies that reduces environmental problems and increases energy efficiency is the storage of solar thermal energy and its consumption upon need. Thermal energy is stored by three methods including sensible thermal energy storage, latent heat storage, and thermochemical heat storage [1-3].

The thermochemical heat storage method has been highly focused on in recent years. This method has high energy storage capacity and the ability to store thermal energy for long time at near ambient temperatures, compared with other thermal energy storage methods. Materials suitable for thermochemical heat storage should have features such as reactivity, redox cycle stability, reversibility, high reaction rates, easy controllability, easy storage, safety, and economic savings [4-6].

Metal oxides are one of the materials groups which have been chosen for thermochemical heat storage applications and are currently undergoing extensive research. Co_3O_4 has shown good redox kinetics in comparison with other metal oxides and recently it been used semi-industrially for solar thermal energy storage [7,8]. Among various oxides for energy storage, cobalt oxide has been shown to be promising thermodynamically due to its high enthalpy and reversibility of the reduction-oxidation process. The possibility for the conversion of CoO and Co_3O_4 oxides into each other during redox reactions could be used to store the thermal energy in this system. The first step of a redox cycle is the endothermic reduction of the Co_3O_4 to CoO at 890°C [9-14] (Eq. (1)).



In the second step of a redox cycle, CoO oxidation occurs when the heat is released (Eq. (2)).



The reduction and re-oxidation reactions of Co_3O_4 /

CoO have reversible potential and the kinetics of the reactions indicates that the reactions are controlled by the rate of heat transfer and diffusion [7]. The kinetically problem of cobalt oxide appears when it is subjected to a lot of redox cycles which results in particles sintering and increasing the oxygen diffusion distance. To overcome this problem, various oxides including Fe_2O_3 , CuO , and Al_2O_3 , etc. have been added to the cobalt oxide. Adding these oxides improves, to some extent, the properties of cobalt oxide thermal energy storage by preventing sintering [15].

To the best knowledge of the authors, the effects of Al_2O_3 and Y_2O_3 additions on cobalt oxide reduction kinetics parameters such as reacted fraction and activation energy have not yet been reported. One of the goals of this research was to study the addition of oxides of metals with the same valence (Al^{3+} and Y^{3+}) but different ionic radius (0.05 nm and 0.09 nm) on the kinetics of Co_3O_4 reduction to CoO . This research obtained very useful background information about the mentioned additives performances on the heat storage properties of Co_3O_4 / CoO pair redox system. In addition, the thermodynamic discussions carried out in this research, although completely theoretical, have not yet been discussed in detail. The thermodynamic discussion of reduction and re-oxidation of the Co_3O_4 / CoO system can lead to a better understanding of the process of thermo-chemical heat storage in a Co_3O_4 / CoO redox pair.

2. Experimental procedure

Cobalt oxide (Co_3O_4 , Merck, >99%, <10 μm), alumina (Al_2O_3 , Fluka, >99%, <10 μm), and yttria (Y_2O_3 , Merck, >99%, <10 μm) were used as raw materials. The first sample was prepared by adding 5 wt% Al_2O_3 to Co_3O_4 (CA) and the second sample was prepared by adding 5 wt% of Y_2O_3 to Co_3O_4 (CY). Then, each sample was ball milled by a high energy planetary ball mill for 2 h (PM100 Retsch) using a 150 ml steel vial and steel balls (10 and 20 mm diameter) under air atmosphere, a ball to powder weight ratio of 20, and a rotation speed of 300 rpm. The samples compositions were selected according to previous research [7,16] as optimum compositions.

Isothermal kinetics studies were performed at 1040, 1060, and 1130°C for the CA sample and at 1060, 1090, and 1130°C for the CY sample to investigate the

effect of secondary oxide (alumina and yttria) addition on the reduction kinetics of Co_3O_4 .

In thermogravimetry experiments, a sample of 3.8 g in an alumina crucible ($10 \times 10 \times 5$ mm) was placed in the hot zone of a furnace (Azar furnace 1250) at a certain temperature, and maintained at that temperature until a very low weight change was observed. During the process, the sample weight was recorded by a digital balance (A&D model EK-600i) connected to a laptop by software (RS weight A&D). More details about the weight recording set up can be found in Ref. [17]. It is notable that the furnace set-point was used for temperature measurements. Scanning electron microscopy (LMU VEGA//TESCAN) was used to investigate the morphology of sample particles.

The reacted fraction (α) at different times and temperatures, which is required to calculate the reduction activation energy, was calculated according to Eq. (3). According to Eq. (1), the maximum theoretical weight loss is close to 6.64 wt% during Co_3O_4 reduction into 3CoO .

$$\alpha = \text{Weight loss (wt\%)} / 6.64 \quad (3)$$

Subsequently, an α curve versus time was depicted for each sample at an isothermal temperature. A model-free method was used to calculate the activation energy. The temperature dependence of the rate constant (k) is usually given by the Arrhenius equation (Eq. (4)) [18]:

$$k = A \exp(-E_a/RT) \quad (4)$$

Where, A is the pre-exponential (frequency) factor, E_a is the activation energy, T is the absolute temperature, and R is the gas constant.

For the integral reaction model the Eq. (5) is used:

$$g(\alpha) = kt \quad (5)$$

Substitution of Eq. (5) into Eq. (4) gives:

$$g(\alpha) = A \exp(-E_a/RT)t \quad (6)$$

The slope of $-\ln t$ versus $1/RT$ for each α , gives E_a according to Eq. (7).

$$-\ln t_\alpha = \ln [A/g(\alpha)]_\alpha - E_{a\alpha}/RT_\alpha \quad (7)$$

3. Results and discussion

3.1. Thermodynamic study of redox reactions of $\text{CoO}/\text{Co}_3\text{O}_4$ system

Due to the reduction experiments being performed in air atmosphere, a thermodynamic study is conducted according to the real conditions. The reduction of Co_3O_4 into CoO and the re-oxidation of CoO to Co_3O_4 took place using thermal energy according to Eqs. (1) and (2). Various references [7,14] refer to the equilibrium temperature of the reduction and re-oxidation of $\text{Co}_3\text{O}_4/\text{CoO}$ as occurring in the range of 890-920°C.

3.1.1. Relationship between Gibb's free energy and temperature

The relationship of Gibb's free energy with T for Co_3O_4 reduction to CoO (Eq. (1)) is given according to Eq. (8) [19,20]. Assuming $a_{\text{CoO}}=1$ and $a_{\text{Co}_3\text{O}_4}=1$, we can write Eq. (8) as Eq. (9).

$$\Delta G = 43800 - 35.4 T + 1.987 T \ln K \quad (\text{cal/mol}), \quad (8)$$

$$K = [(a_{\text{CoO}}^3 \cdot P_{\text{O}_2}^{1/2}) / a_{\text{Co}_3\text{O}_4}]$$

$$\Delta G = 43800 - 35.4 T + 0.9935 T \ln P_{\text{O}_2} \quad (\text{cal/mol}) \quad (9)$$

where, T is the temperature in Kelvin, K is the reaction constant, P_{O_2} is the partial pressure of oxygen in air atmosphere and ΔG is the Gibb's free energy in cal/mol. If the reduction and re-oxidation reactions are carried out in the air and partial oxygen pressure is assumed to be 0.21 atm, Eq. (9) will be as follows:

$$\Delta G = 43800 - 35.4 T + 0.9935 T \ln(0.21)$$

$$= 43800 - 36.95 T \quad (\text{cal/mol}) \quad (10)$$

$$\text{or } \Delta G = 43.8 - 0.037 T \quad (\text{kcal/mol})$$

Fig. 1 presents Eq. (10) as a curve. It is possible to study the effect of reduction temperature on Gibb's free energy in more detail. As shown in Fig. 1, increasing the temperature reduces the Gibb's free energy of the Co_3O_4 reduction to CoO . This means that increasing the reaction temperature above the equilibrium temperature (912.23 °C or 1185.38 K) makes the reduction reaction thermodynamically more favorable, while it makes the re-oxidation reaction thermodynamically undesirable.

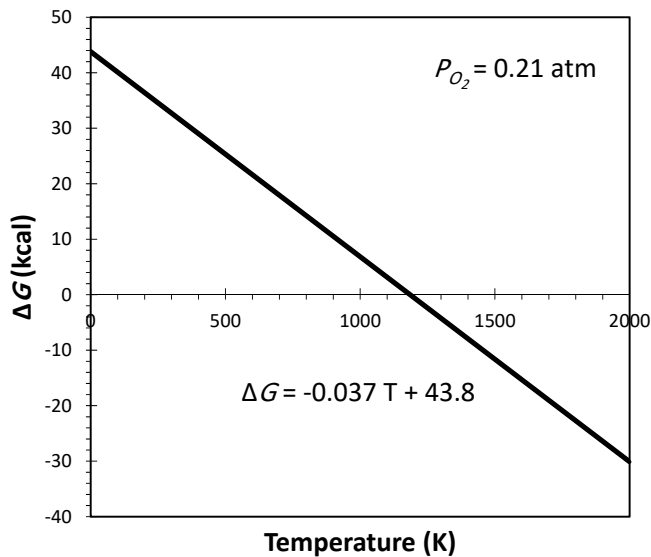


Fig. 1. Relationship between reduction ΔG and temperature under air atmosphere ($P_{O_2} = 0.21$ atm).

3.1.2. Relation between ΔG and oxygen P_{O_2}

By putting Eq. (10) equal to zero, T_e of the Co_3O_4 reduction to CoO can be calculated at atmospheric air pressure ($P_{O_2} = 0.21$ atm):

$$\Delta G = 43800 - 36.95 T = 0 \quad (11)$$

$$\rightarrow T_e = 1185.38K = 912.23^\circ C$$

Putting the equilibrium temperature ($912.23^\circ C$) into Eq. (9), we obtain the following equation:

$$\Delta G = 43800 - 35.4 T + 0.9935 T \ln P_{O_2} \quad (12)$$

$$\rightarrow \Delta G = 1837.548 + 1177.675 \ln P_{O_2}$$

Fig. 2 presents the relationship between ΔG and P_{O_2} at T_e ($912.23^\circ C$). This means that with a decrease in the P_{O_2} at T_e , the value of ΔG of reduction reduces. In other words, by reducing the partial pressure of oxygen, the Co_3O_4 reduction into CoO will thermodynamically be more favorable. Also, Fig. 2 shows that P_{O_2} variations at lower values (less than 0.2 atm) are more effective in changing the reduction ΔG .

3.1.3. Relationship between T_e and P_{O_2}

If we put $\Delta G=0$ in Eq. (8), the relation between T_e and P_{O_2} , Eq. (13), appears as seen in Fig. 3.

$$43800 - 35.4 T \ln P_{O_2} = 0 \rightarrow T_e = 1237 (P_{O_2})^{0.027} \quad (13)$$

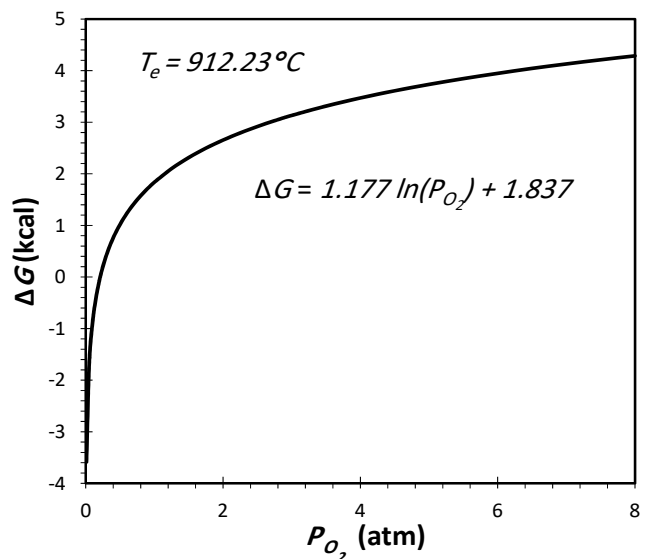


Fig. 2. Relationship between ΔG and P_{O_2} .

According to Fig. 3, increasing the partial pressure of oxygen in the reaction environment increases the equilibrium temperature of Co_3O_4 reduction into CoO and vice versa. The equilibrium temperature under atmospheric pressure ($P_{O_2} = 0.21$ atm) is close to 1185 K ($912^\circ C$), while increasing the oxygen partial pressure to 1 atm increases the equilibrium temperature close to 1237 K ($964^\circ C$). This means that by increasing the oxygen partial pressure up to five fold (from 0.2 to 1 atm), the equilibrium temperature increase is only 52 K. Also, increasing the P_{O_2} from 2 to 5 atm changes the equilibrium temperature from 1262 K to 1296 K. In general, it can be said that at low pressures of oxygen (less than 0.2 atm), the effect of the partial pressure of oxygen on the equilibrium temperature is

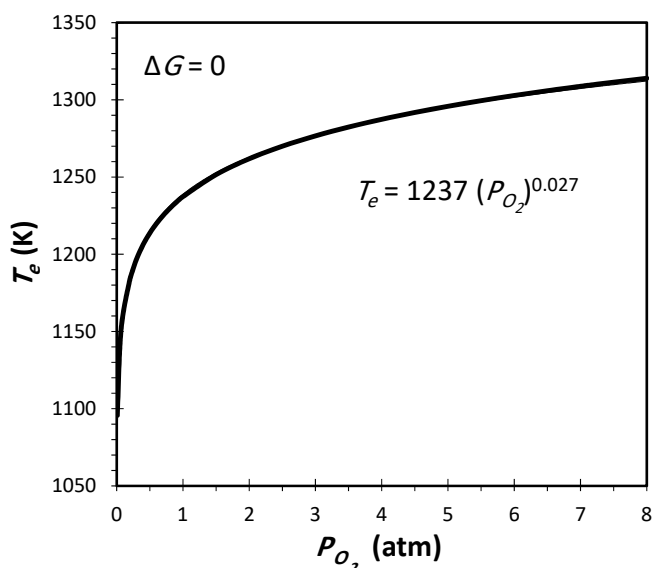


Fig. 3. Relationship between T_e and P_{O_2} .

high, while at pressures above 0.2 atm, the effect of partial pressure on the equilibrium temperature is low.

3.2. Kinetic studies and calculation of reduction activation energy

Figures 4 and 5 show the weight loss of CA and CY samples during reduction at various isothermal temperatures. According to Fig. 4, an increase in the reduction temperature from 1060 to 1130°C increases the total oxygen desorption from 2.6 to 3.5 wt% after 6 minutes. However, as shown in Fig. 5, with an increase in the reduction temperature from 1060 to 1130°C, the oxygen desorption value in the CY sample increases from 1.4 to 2 wt%. It is clear that, in similar conditions, the oxygen desorption from the CY sample is lower than from the CA sample. Thus, the sample containing alumina exhibits a better performance than the sample containing yttria in view of oxygen desorption.

Reacted fraction variations with time at different temperatures for the CA and CY samples are shown in Figures 6 and 7, respectively. As shown in Fig. 6, the ultimate reacted fraction of the CA sample at 1040, 1060, and 1130°C after 6 minutes is close to 0.37, 0.40 and 0.55, respectively. This is in accordance with the thermodynamic studies in Fig. 1 which show that at low temperatures the reduction reaction is unfavorable.

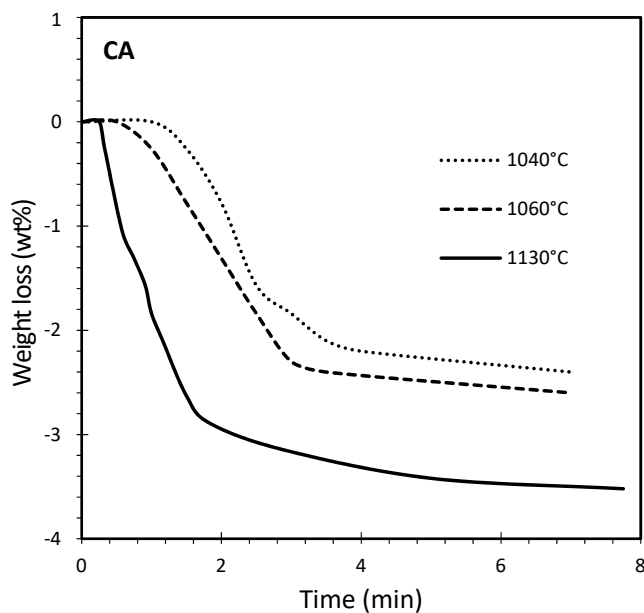


Fig. 4. Weight loss of CA sample at three isothermal temperatures of 1040, 1060 and 1130°C.

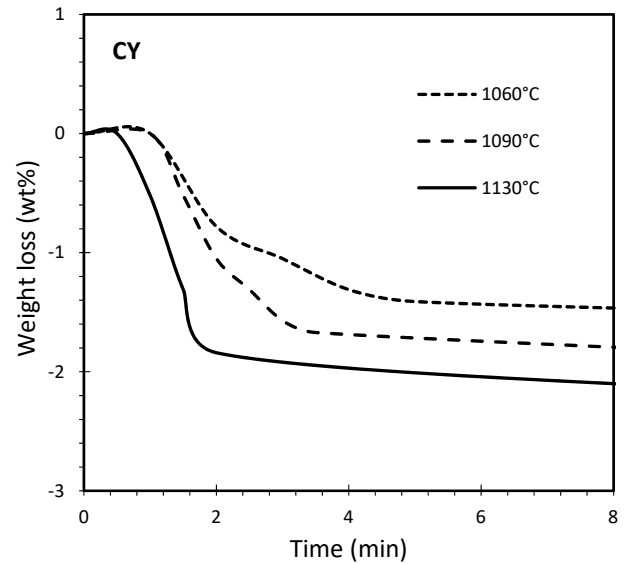


Fig. 5. Weight loss of CY sample at three isotherm temperatures of 1060, 1090, and 1130°C.

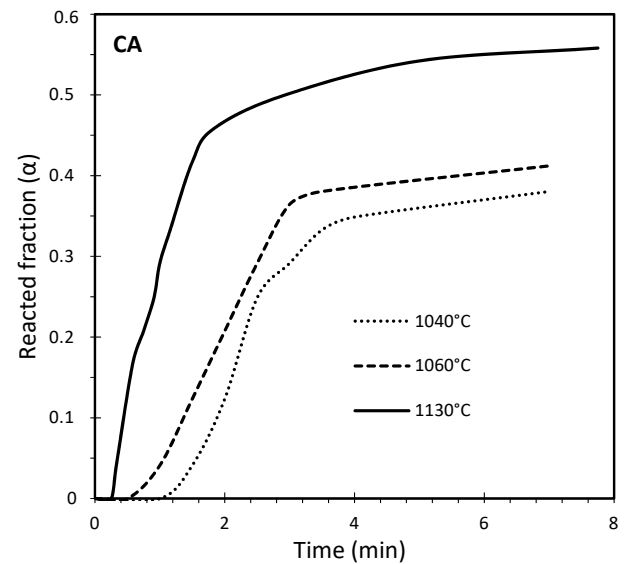


Fig. 6. Reacted fraction (α) versus time in CA reduction reaction

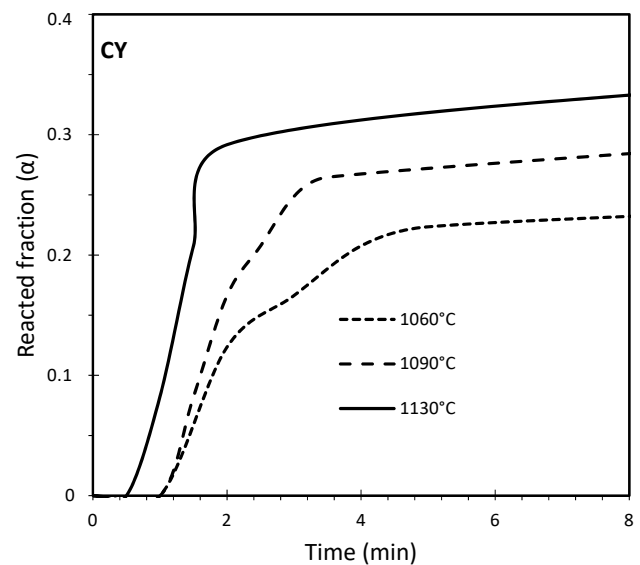


Fig. 7. Reacted fraction (α) versus time in CY reduction reaction.

Reacted fraction values obtained for the CY samples are less than that for the CA samples. As shown in Fig. 7, the ultimate reacted fraction of the CY sample after 6 minutes is close to 0.22, 0.27, and 0.33 at 1060, 1090, and 1130°C, respectively.

Figures 8 and 9 show the curves of $-\ln t$ versus $1/RT$ related to the CA and CY samples, respectively. Slope of these curves is equal to $-E_a$ according to Eq. (7). As can be seen in these curves, by changing the α value the slope of lines changes which means the activation energy changes with the α variation. It is clear that the reduction activation energy change is different for the CA and CY samples. Activation energy values derived from Figures 8 and 9, were plotted in Fig. 10. In addition, reduction activation energy of as-received cobalt oxide [21] was also depicted in Fig. 10 for comparison.

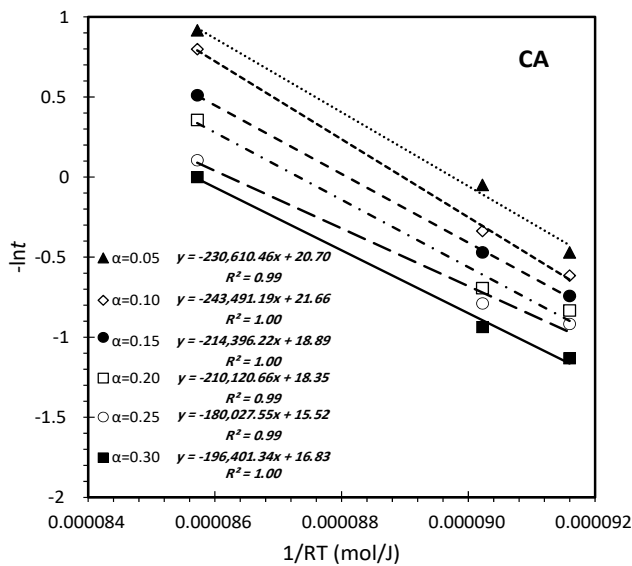


Fig. 8. $-\ln t$ versus $1/RT$ for CA sample.

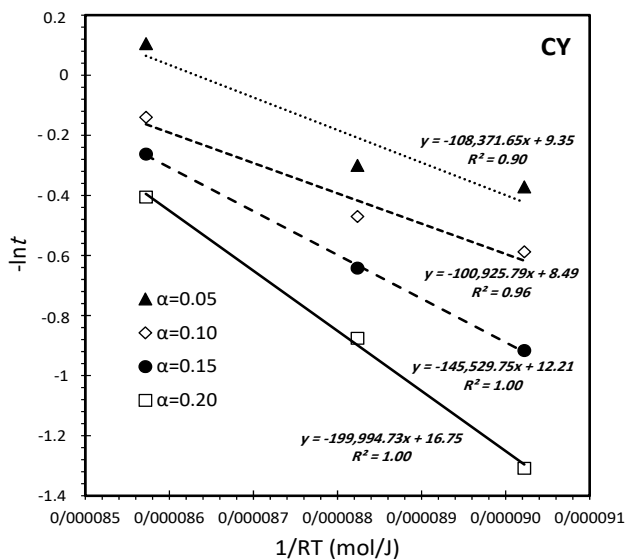


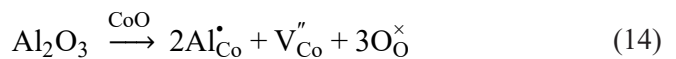
Fig. 9. $-\ln t$ versus $1/RT$ for CY sample.

The difference in the performance of alumina and yttria on the reduction of cobalt oxide can be related to their ionic radii difference [7], ability to create new compounds having different decomposition temperatures [15,21,22], and their different effects on the sintering of cobalt oxide particles [7,15-17,21,22]. The effect of these parameters will be discussed later.

Comparing the curves in Fig. 10 demonstrates that reduction activation energy of the CY sample up to $\alpha=0.15$ is lower than or equal to the reduction activation energy of as-received cobalt oxide, while it is higher than for α values more than 0.15. In the case of the CA sample, it is clear that reduction activation energy is always greater than the reduction activation energy of as-received cobalt oxide up to $\alpha = 0.30$.

In addition, according to Fig. 10, the reduction activation energy of as-received cobalt oxide increased with a slight slope when the reacted fraction increased, while the reduction activation energy of CA and CY samples decreased and increased, respectively, as the reacted fraction increased. One of the reasons for the difference in reduction activation energies for CA, CY, and as-received Co_3O_4 relates to different sintering level of particles in the mentioned samples. Fig. 11 presents the SEM images of the CA and CY samples. Reasons for the differences in the behavior of CA and CY samples in view of oxygen desorption (Figures 4 and 5) and reduction activation energy (Fig. 10) are discussed in the following section.

CA sample behavior: Incorporation of Al_2O_3 into the CoO lattice during ball milling and reduction processes brings a positive charge into the lattice that should be neutralized by introducing Co vacancies. The corresponding defect reaction using the Kroger-Vink notation is as follows (Eq. (14):



The produced vacancies in the structure facilitate the oxygen diffusion. Decline in the reduction activation energy of CA can be due to the continuous diffusion of Al^{3+} ions into the cobalt oxide structure by the advancement of the reduction reaction resulting in the production of more vacancies.

CY sample behavior: Y^{3+} ions unlike Al^{3+} ions cannot easily be introduced into the structure of cobalt oxide due to the large ionic radius (Table 1). While, cobalt ions can be introduced into the structure of yttrium

oxide. This happens during mechanical activation and reduction process. As a result, a number of vacancies in the structure of cobalt oxide arise and its structure in terms of electrical charge balance is faced with a lack of positive charges or an abundance of negative charge. To maintain the balance of electrical charge in the structure, a number of oxygen anions are readily released from the cobalt oxide structure and make many vacancies in the structure resulted in better oxygen diffusion. For this reason, in lower α values the reduction activation energy of CY is lower. However, with the progression of the oxygen desorption reaction (reduction) and achieving an electrical balance by the structure, its behavior returns to normal, so that its behavior is similar to the behavior of the as-received cobalt oxide at $\alpha = 0.15$ and is similar to the behavior of CA sample at $\alpha = 0.20$. As the reaction progresses (increase in α), oxygen desorption from CY becomes more difficult due to the very positive effect of yttrium oxide on sintering of cobalt oxide particles and the subsequent kinetic problem in oxygen desorption from the structure. That is why the reduction activation energy of the CY sample increases suddenly beyond $\alpha = 0.10$.

As-received cobalt oxide behavior: Due to a lack of secondary oxide phase in this sample (alumina and yttria), there is no discussion similar to CA and CY samples and the reduction activation energy increases at a low rate as the α value increases. The increase in activation energy as the α value increases is only due to sintering of cobalt oxide particles during the reduction process [15-17,21,22].

According to the above discussion, the reasons for differences in the behavior of the samples in terms of oxygen desorption and activation energy can be summarized as follows:

a-Difference in ionic radius: according to Table 1, the Al^{3+} ionic radius (0.05 nm) is smaller than the Y^{3+}

ionic radius (0.09 nm); therefore, Al^{3+} ions, unlike Y^{3+} ions, can easily be replaced with $\text{Co}^{2+}/\text{Co}^{3+}$ ions in the structure of Co_3O_4 ($\text{Co}_2\text{O}_3 \cdot \text{CoO}$). Although the behavior of Al^{3+} and Y^{3+} ions are not the same, the same result (creating vacancies) arises from their behavior. In the yttria-containing sample, cobalt ions migration into the yttria structure is dominant and leaves more vacancies in the structure of cobalt oxide. Moreover, the abundance of negative charges created by that, facilitates the oxygen desorption (exit the oxygen anions) to achieve an electrical charge balance in the cobalt oxide structure. For this reason, at lower α values (before sintering of CY sample), the reduction activation energy of CY is less than CA.

b-Ability to create new compounds: formation of compounds between cobalt oxide and alumina/yttria, which have high decomposition temperatures, reduce the sorption capacity of the CA and CY samples. But, the decomposition temperature of the new compounds in cobalt oxide-alumina and cobalt oxide-yttria systems are different. This has been proven by the findings of other researchers [15-17].

c-Effect on sintering of cobalt oxide particles: sintering of the cobalt oxide particles is a key parameter in the decline of oxygen desorption. The coarse particles increase the diffusion distance of oxygen atoms and increase the time required for the reduction process [7]. According to SEM images (Fig. 11), it is also clear that in the case of yttrium oxide as an additive, particle sintering is much more than that of aluminum oxide as an additive.

Table 1. Lattice parameters of compounds and ion radius of Co^{2+} , Co^{3+} , Al^{3+} , O^{2-} , and Y^{3+} [23,24].

| Compound | Lattice parameter (nm) | Ion | Ionic radius (nm) |
|-------------------------|------------------------|------------------|-------------------|
| Co_3O_4 | 0.8084 | Co^{3+} | 0.06 |
| CoO | 0.4260 | Co^{2+} | 0.07 |
| Al_2O_3 | a=0.4785 and c=1.2991 | Al^{3+} | 0.05 |
| Y_2O_3 | 1.062 | Y^{3+} | 0.09 |
| --- | --- | O^{2-} | 0.14 |

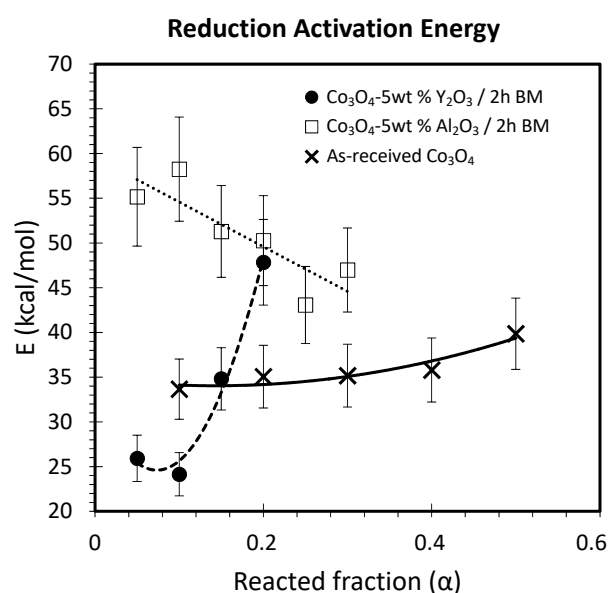


Fig. 10. The calculated activation energy as reduction reacted fraction for the as-received cobalt oxide, CA and CY. (data of as-received Co_3O_4 was taken from ref. [21])

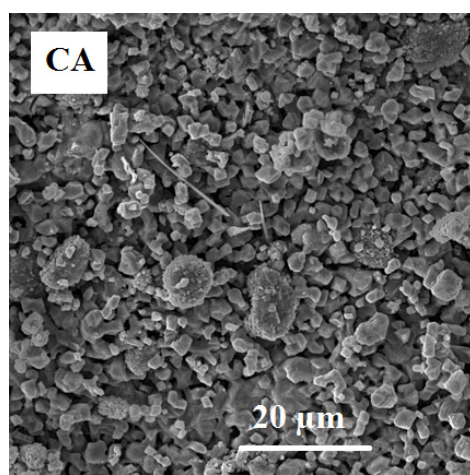
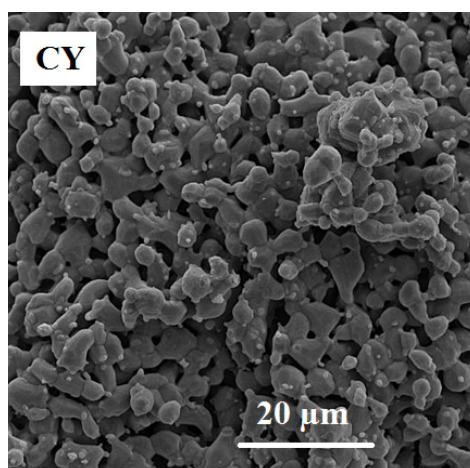


Fig. 11. SEM images of CA and CY samples after redox.

As previously stated, the sintering increases the oxygen diffusion distance resulting in long reduction reaction times. The isothermal TG curves in Fig. 5 confirm a lower weight loss of Co_3O_4 - 5wt% Y_2O_3 composite than that of Co_3O_4 - 5wt% Al_2O_3 .

4. Conclusions

Increasing the reaction temperature to more than the equilibrium temperature (912.23°C) makes the reduction reaction thermodynamically more favorable. Also, a decrease in the partial pressure of oxygen at a given temperature reduces the Gibb's free energy of reduction process and improves the Co_3O_4 reduction into CoO thermodynamically. Moreover, increasing the partial pressure of oxygen in the reaction environment increases the equilibrium temperature of Co_3O_4 reduction into CoO . The required Activation energy for reduction of the CA and CY samples, depending on the reacted fraction value, is in the range of 40-65 kcal/mol and 25-50 kcal/mol, respectively. The reduction activation

energy of the CA sample is reduced by increasing the reacted fraction and the activation energy of the CY sample increases by increasing the reacted fraction. The reduction activation energy of as-received Co_3O_4 is increased by a slight slope by increasing the reacted fraction (35-40 kcal/mol). The difference in the performance of aluminum oxide and yttrium oxide on the reduction of cobalt oxide is due to their ionic radii difference, the ability to create new compounds with different decomposition temperatures, and their different effect on the sintering of cobalt oxide particles.

Acknowledgments

The author's would like to thank Mr. A. Nsari for his assistance during the experiments. This work was supported by the Hamedan University of Technology [Grant No. 18-94-1-361].

References

- [1] J.E. Raßthl, T.E. Drennen, Pathways to a hydrogen future, 3rd ed., Elsevier, London, 2007.
- [2] D. Rahm, Sustainable energy and the states, essay on politics markets and leadership, 1st ed., McFarland, North Carolina, 2002.
- [3] A.H. Abedin, A critical review of thermochemical energy storage, The open Renewable Energy, 4 (2011) 42-46.
- [4] Thermal energy storage. 2013. Available from: [http:// www.irena.org/publications](http://www.irena.org/publications).
- [5] G. Karagiannakis, C. Pagkoura, E. Halevas, P. Baltzopoulou, A.G. Konstandopoulos, Cobalt/cobaltous oxide based honeycombs for thermochemical heat storage in future concentrated solar power installations, Sol. Energy, 133 (2016) 394-407.
- [6] D. Lefebvre, F.A. Tezel, A review of energy storage technologies with a focus on adsorption thermal energy storage processes for heating applications, Renew. Sußt.. Energ. Rev. 67 (2017) 116-125.
- [7] U.S. Department of Energy, Thermochemical heat storage for concentrated solar power, General atomic project 30314, 2008.
- [8] A. Carrillo, J. Moya, A. Bayon, P. Jana, V.A. de la Pena O Shea, M. Romero, J. Gonzalez-Aguilar, D.P. Serrano, P. Pizarro, J.M. Coronado, Thermochemical energy storage at high temperature via redox cycles

- of Mn and Co oxides: Pure oxides versus mixed oxides, *Sol. Energ. Mat. Sol. C.* 123 (2014) 47-57.
- [9] M. Neises, S. Tescari, L. de Oliveira, M. Roeb, C. Sattler, B. Wong, Solar-heated rotary kiln for thermochemical energy storage, *Sol. Energy*, 86 (2012) 3040-3048.
- [10] A.D. Pelton, H. Schmalzried, J. Sticher, Thermodynamics of Mn_3O_4 - Co_3O_4 , Fe_3O_4 - Mn_3O_4 , and Fe_3O_4 - Co_3O_4 spinels by phase diagram analysis, *Phys. Chem.* 83 (1979) 241-252.
- [11] G.M. Kale, S.S. Pandit, K.T. Jacob, Thermodynamics of cobalt (II,III)-oxide (Co_3O_4) - Evidence of phase-transition, *T. Jpn. I. Met.* 29 (1988) 125-132.
- [12] C.W. Tang, C.B. Wang, S.H. Chien, Characterization of cobalt oxides studied by FT-IR, Raman, TPR and TG-MS, *Thermochim. Acta*, 473 (2008) 68-73.
- [13] K.N. Hutchings, M. Wilson, P.A. Larsen, R.A. Cutler, Kinetic and thermodynamic considerations for oxygen absorption/desorption using cobalt oxide, *Solid State Ionics*, 177 (2006) 45-51.
- [14] A.G. Schrader, A.P. Muroyama, P.G. Loutzenhiser, Solar electricity via an Air Brayton cycle with an integrated two-step thermochemical cycle for heat storage based on Co_3O_4/CoO redox reactions II: Kinetic analyses, *Sol. Energy*, 122 (2015) 409-418.
- [15] T. Block, N. Knoblauch, M. Schmucker, The cobalt-oxide/iron-oxide binary system for use as high temperature thermochemical energy storage material, *Thermochim. Acta*, 577 (2014) 25-32.
- [16] A. Hsanvand, MSc Thesis, Study of synergistic effect of mechanical activation and Al_2O_3 and Y_2O_3 addition on the thermochemical heat storage properties cobalt oxide, Department of Materials Engineering, Hamedan University of Technology, 2018.
- [17] N. Nekokar, M. Pourabdoli, A. Ghaderi Hamidi, D. Uner, Effect of mechanical activation on thermal energy storage properties of Co_3O_4/CoO system, *Adv. Powder Technol.* 2 (2018) 333-340.
- [18] A. Khawam, D.R. Flanagan, Basics and applications of solid state kinetics, a pharmaceutical perspective, *J. Pharm. Sci.* 95 (2006) 472-498.
- [19] O. Kubaschewski, C.B. Alcock, Metallurgical Thermochemistry, 5th ed., Pergamon Press, Toronto, 1979.
- [20] D.R. Gaskell, Introduction to the Thermodynamics of Materials, 4th ed., Taylor & Francis, New York, 2003.
- [21] N. Nekokar, MSc Thesis, Effect of high energy milling on reduction and oxidation process in Co_3O_4 - Fe_2O_3 system for thermochemical heat storage, Department of Materials Engineering, Hamedan University of Technology, 2017.
- [22] N. Nekokar, M. Pourabdoli, A. Ghaderi Hamidi, Effects of Fe_2O_3 addition and mechanical activation on thermochemical heat storage properties of the Co_3O_4/CoO system, *J. Part. Sci. Technol.* 4 (2018) 13-22.
- [23] O.D. Neikov, S. Naboychenko, Handbook of Non-Ferrous Metal Powders, 1st ed., Elsevier, 2008.
- [24] Y. Mao, J. Engels, A. Houben, M. Rasinski, J. Steffens, A. Terra, Ch. Linsmeier, J.W. Coenen, The influence of annealing on yttrium oxide thin film deposited by reactive magnetron sputtering: Process and microstructure, *Nucl. Mater. Energy*, 10 (2017) 1-8.